

Excitonic Instability at the Spin-State Transition in the Two-Band Hubbard Model

Jan Kuneš and Pavel Augustinský¹

¹*Institute of Physics, Academy of Sciences of the Czech republic,
Cukrovarnická 10, Praha 6, 162 53, Czech Republic*

(Dated: February 6, 2018)

Using linear response theory with the dynamical mean-field approximation we investigate the particle-hole instabilities of the two-band Hubbard model in the vicinity of the spin-state transition. Besides the previously reported high-spin–low-spin order we find an instability towards triplet excitonic condensate. We discuss the strong and weak coupling limits of the model, in particular, a connection to the spinful hard-core bosons with a nearest-neighbor interaction. Possible realization in LaCoO₃ at intermediate temperatures is briefly discussed.

PACS numbers: 71.35.Lk, 71.27.+a, 05.30.Jp, 75.45+j

I. INTRODUCTION

Search for new states of matter is one of the central topics of condensed matter physics. While the development of cold atom techniques allowed the construction of many exotic phases in particular in systems of interacting bosons, electronic order parameters other than spin, charge and orbital densities or s-wave pairing superconductivity are rather rare in real materials. We report observation of an off-diagonal order close to the spin-state transition in the two-band Hubbard model with Hund's coupling and show that such electronic system provides realization of some of the phases observed with interacting bosons.

The role of Hund's coupling in correlated electron systems has been recently theoretically studied in the context of Hund's metals^{1,2} and the spin-state transitions driven by pressure^{3,4} as well as temperature^{5,6} or doping⁷. Competition of different spin states was also linked to the peculiar magnetic properties of iron pnictides⁸. The two-band Hubbard model at half filling provides a minimal lattice realization of the spin-state transition in correlated electron systems^{9,10}. Recently, a reentrant transition of Ising type to a two-sublattice order of high-spin (HS) and low-spin (LS) states was reported on a bipartite lattice in the vicinity of the spin-state transition¹¹. It was proposed that such ordered state can explain properties of the notorious spin-state transition compound LaCoO₃ at intermediate temperatures.

In this article, we report a systematic investigation of the particle-hole instabilities in the normal phase of the two-band Hubbard model. Besides the previously reported Ising instability we find that an excitonic instability which breaks a continuous symmetry dominates over a broad range of parameters. The idea of an instability due to the long-range part of the Coulomb interaction in small gap semiconductors leading to so the called excitonic insulator phase appeared fifty years ago¹² and more recently was applied to the physics of LaB₆¹³. Following the work of Batista¹⁴ on electronic ferroelectricity, the excitonic instability was studied in the extended Falicov-Kimball model^{15–17} as well as the two-band Hub-

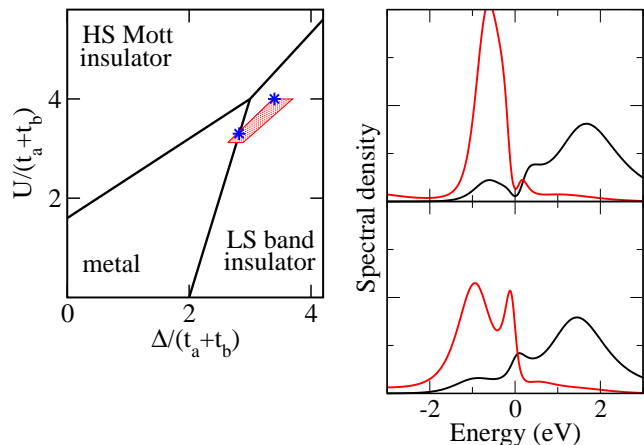


FIG. 1: (color online) Left: the conceptual phase diagram of the two-band Hubbard model for $U = 4J$. The shaded area marks the parameter range visited while varying the band asymmetry ζ and crystal field Δ . Right: 1P spectral densities obtained at the points marked by stars (upper panel corresponds to the upper star) at temperatures just above the leading T_c .

bard model without Hund's coupling^{18,19}.

The connection to the bosonic physics arises in the strong-coupling limit. As was shown by Batista¹⁴, the extended Falicov-Kimball model at half filling maps onto spinless hard-core bosons with nn repulsion, a problem much studied in the context of solid, superfluid and possibly a supersolid phase^{20,21}. We show that in the strong-coupling limit of the two-band Hubbard model with Hund's coupling the mapping generalizes to the spinful hard-core bosons with some additional nn terms, a much less studied problem^{22,23} with a rich phase diagram.

The paper is structured as follows. In Section II we state the problem and describe the computational method. In Section III we summarize our numerical results. In Section IV we derive the strong- and weak-coupling limits of the studied model in order to elucidate the nature of the instabilities reported in Section III. We

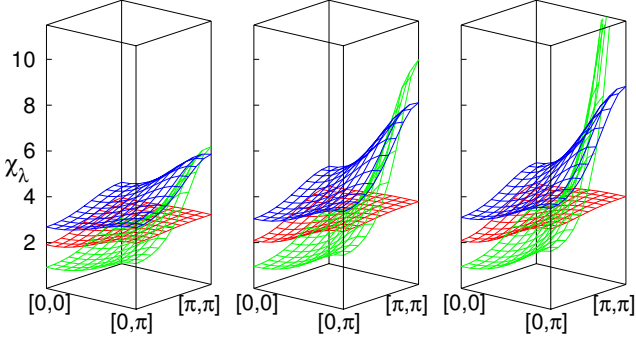


FIG. 2: (color online) The typical \mathbf{q} -dependence of the leading eigenvalues of the susceptibility matrix: spin longitudinal (red), OD (green) and OO (blue) in a system with a large band asymmetry $\zeta = 0.22$, $\Delta = 3.40$ at temperatures 773 K, 644 K and 580 K (left to right).

briefly discuss the classical limit, which provides the simple understanding of the HS-LS phase, and then focus on various aspects of the excitonic phase. In Section V we summarize our main findings.

II. COMPUTATIONAL PROCEDURE

We consider the two-band Hubbard model with nearest-neighbor (nn) hopping on a bipartite (square) lattice with the kinetic H_t and the interaction $H_{\text{int}} = H_{\text{int}}^{\text{dd}} + H'_{\text{int}}$ terms given by

$$\begin{aligned}
 H_t &= \frac{\Delta}{2} \sum_{i,\sigma} (n_{i\sigma}^a - n_{i\sigma}^b) + \sum_{i,j,\sigma} (t_a a_{i\sigma}^\dagger a_{j\sigma} + t_b b_{i\sigma}^\dagger b_{j\sigma}) \\
 &\quad + \sum_{\langle ij \rangle, \sigma} (V_1 a_{i\sigma}^\dagger b_{j\sigma} + V_2 b_{i\sigma}^\dagger a_{j\sigma} + c.c.) \\
 H_{\text{int}}^{\text{dd}} &= U \sum_i (n_{i\uparrow}^a n_{i\downarrow}^a + n_{i\uparrow}^b n_{i\downarrow}^b) + (U - 2J) \sum_{i,\sigma} n_{i\sigma}^a n_{i-\sigma}^b \\
 &\quad + (U - 3J) \sum_{i\sigma} n_{i\sigma}^a n_{i\sigma}^b \\
 H'_{\text{int}} &= J \sum_{i\sigma} a_{i\sigma}^\dagger b_{i-\sigma}^\dagger a_{i-\sigma} b_{i\sigma} + J' \sum_i (a_{i\uparrow}^\dagger a_{i\downarrow}^\dagger b_{i\downarrow} b_{i\uparrow} + c.c.).
 \end{aligned} \tag{1}$$

Here $a_{i\sigma}^\dagger, b_{i\sigma}^\dagger$ are the creation operators of fermions with spin $\sigma = \uparrow, \downarrow$ and $n_{i\sigma}^c = c_{i\sigma}^\dagger c_{i\sigma}$. Symbol $\sum_{i,j}$ implies summation over ordered nn pairs, while $\sum_{\langle ij \rangle}$ implies summation over nn bonds (pairs without order). The model is studied at half filling, two electrons per site on average. The crystal field Δ and the Hund's exchange J are chosen so that the system is in the vicinity of the LS-HS transition.

The numerical calculations were performed in the dynamical mean-field approximation^{24,25} with the density-density interaction $H_{\text{int}}^{\text{dd}}$ only. The effect of adding H'_{int}

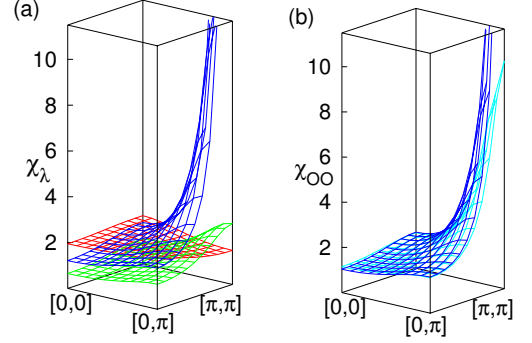


FIG. 3: (color online) Left: Leading eigenvalues for equal bandwidths ($\zeta = 1$) and $\Delta = 3.40$ eV at 1160 K. The blue OO mode diverges faster than the green OD mode. Right: Splitting of the OO mode from (b) due to added cross-hopping $V_{1,2} = 0.1$ eV. The leading mode (two-fold degenerate) has the form $a_\sigma^\dagger b_{-\sigma} + b_\sigma^\dagger a_{-\sigma}$ with $\sigma = \uparrow, \downarrow$.

is considered in Section IV. We use the hybridization expansion continuous time quantum Monte Carlo (CT-HYB)^{26,27} to solve the auxiliary impurity problem and obtain the local one-particle (1P) and two-particle (2P) propagators. For selected parameters we have benchmarked the CT-HYB results against those obtained with the Hirsch-Fye implementation of the present procedure¹¹.

In order to study phase transitions, we search numerically for divergent static particle-hole susceptibilities in the disordered high temperature phase. The lattice susceptibility $\chi_{\alpha\beta,\gamma\delta}(T, \mathbf{q})$ is a \mathbf{q} -dependent matrix function indexed by pairs of spin-orbital indices. It is calculated from the Bethe-Salpeter equation as a function of the full 1P propagator and the 2P-irreducible vertex. The crucial DMFT simplification consists in the fact that the 2P irreducible vertex is \mathbf{k} -independent and equals the impurity 2P irreducible vertex²⁴. Therefore the momentum dependence of $\chi(T, \mathbf{q})$ comes entirely from the 1P propagator.

We calculate $\chi(T, \mathbf{q})$ on dense \mathbf{q} -mesh in the Brillouin zone, diagonalize for every \mathbf{q} , and identify the largest eigenvalues with the corresponding eigenvectors. The transition temperature is obtained from the zero crossing $\chi_\lambda^{-1}(T_c) = 0$ of the inverse of the largest eigenvalue $\chi_\lambda^{-1}(T, \mathbf{q}) = 0$. The advantage of this approach is that no prior assumptions about the symmetry of the ordered phase is needed.

III. NUMERICAL RESULTS

In this section we present the DMFT results obtained for the Hamiltonian $H_t + H_{\text{int}}^{\text{dd}}$. Following Ref. 11, we set $U=4, J=1$ and use eV as energy units to allow for a straightforward comparison. The basic phase diagram of model (1) at half filling was computed by Werner and

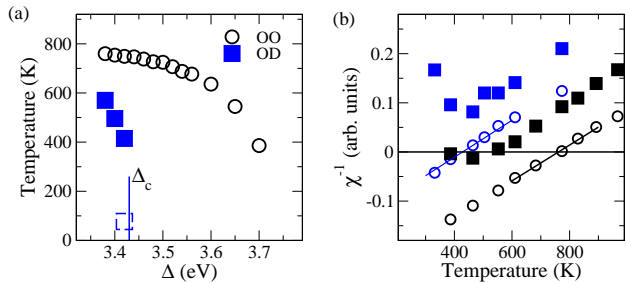


FIG. 4: (color online) (a) Representative dependencies of the instability temperatures on the crystal field Δ : T_{OD} (squares) for $\zeta = 0.28$ and T_{OO} (circles) for $\zeta = 0.55$. The open square marks the position of the reentrant transition taken from Ref. 11. The blue line marks the estimated position of Δ_c . (b) The T -dependence of the inverse eigenvalues χ_{OO}^{-1} (circles) and χ_{OD}^{-1} (squares) of the susceptibility at selected values of Δ . The parameters $\zeta = 0.28$, $\Delta = 3.44$ eV (blue) correspond to $\Delta \gtrsim \Delta_c$ where the OD instability already disappeared. For $\zeta = 0.55$, $\Delta = 3.38$ eV (black) the OD instability exists only in a finite interval of temperatures. In both cases the OO is the leading instability, which is physically realized.

Millis⁹ and its cartoon version is presented in Fig. 1. We are interested in a small region close to the boundary between HS Mott insulator and LS band insulator, which fixes the Δ of interest to $3J$ approximately. Our main variable parameter will be the asymmetry between a and b derived band characterized by $\zeta = \frac{2t_a t_b}{t_a^2 + t_b^2}$. For reason that becomes apparent in the discussion of the strong coupling limit, we choose to vary ζ while keeping the sum $t_a^2 + t_b^2$ fixed. Consequently, the point representing our system moves slightly, covering the red region of Fig. 1 when going between symmetric bands, $\zeta = 1$, and the flat-band limit, $\zeta = 0$.

First, we discuss the eigenmodes of $\chi(\mathbf{q})$ for $t_a = 0.45$ eV, $t_b = 0.05$ eV ($\zeta = 0.22$), $V_{1,2} = 0$, and $\Delta = 3.40$ eV, the parameters of Ref. 11. The full 16×16 matrix of $\chi(\mathbf{q})$ can be, in a standard way using the spin-conservation law, block-diagonalized to $\uparrow\uparrow - \downarrow\downarrow$, $\uparrow\uparrow + \downarrow\downarrow$, $\uparrow\downarrow$ and $\downarrow\uparrow$ blocks (channels), each having 4×4 orbital structure. We find three distinct branches of $\chi_\lambda(\mathbf{q})$ with sizable magnitude. These correspond to i) the spin longitudinal mode $\sum_\sigma \sigma(n_\sigma^a + n_\sigma^b)$ in the $\uparrow\uparrow - \downarrow\downarrow$ channel, ii) the orbital diagonal (OD) mode $\sum_\sigma (n_\sigma^a - n_\sigma^b)$ in the $\uparrow\uparrow + \downarrow\downarrow$ channel, and iii) four degenerate orbital off-diagonal (OO) modes $a_\uparrow^\dagger b_\downarrow$, $b_\uparrow^\dagger a_\downarrow$, $a_\downarrow^\dagger b_\uparrow$, $b_\downarrow^\dagger a_\uparrow$ in the $\uparrow\downarrow$ and $\downarrow\uparrow$ channels. In Fig. 2, the \mathbf{q} dependence of the corresponding eigenvalues in the 2D Brillouin zone is plotted for several temperatures. Similar plot for symmetric bands, $\zeta = 1$, is shown in Fig. 3.

The leading instability for $\zeta = 0.22$ is identified in the OD mode at (π, π) . The corresponding transition temperature agrees well with the onset of the HS-LS checkerboard order found in Ref. 11. Increasing the crystal field Δ rapidly suppresses the transition temperature T_{OD} , see Fig. 4a, and the OD instability eventually disappears

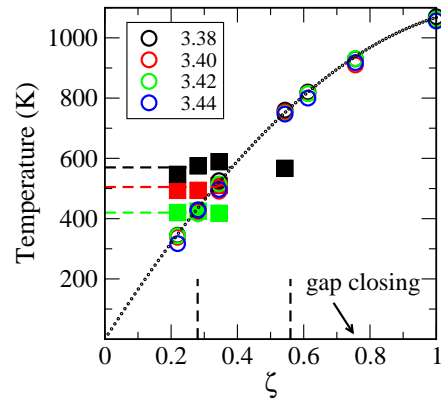


FIG. 5: (color online) Instability of the normal phase as a function of band asymmetry ζ for various CF parameters Δ . Open circles denote the divergence T_{OO} of the OO mode, filled squares mark the divergence T_{OD} of the OD mode. The lines are guides to the eye. The dashed vertical lines mark the ζ 's for which the Δ dependences of T_{OO} and T_{OD} are shown in Fig. 4a.

above some Δ_c . For $\Delta \lesssim \Delta_c$ the OD instability disappears at low temperatures as shown in Fig. 4b, leading to a reentrant transition. For $\Delta \gtrsim \Delta_c$, the proximity of the ordered phase at an intermediate temperature gives rise to a peak in the susceptibility, Fig. 4b. These results provide the same picture as the calculations of Ref. 11 performed in the ordered HS-LS phase. However, in addition to that, one can see that the OO susceptibility also exhibits a substantial increase at (π, π) with decreasing temperature.

Next, we vary the band asymmetry ζ while keeping the cross-hopping $V_{1,2} = 0$. For more symmetric bands a different result is obtained, as shown in Fig. 3, where the dominant $\chi_\lambda(\mathbf{q})$ are plotted for $\zeta = 1$. In this case, the OO mode at (π, π) is the leading instability. This implies formation of an ordered state with spontaneous local off-diagonal hybridization characterized by non-zero value of $\langle a_{i,\sigma}^\dagger b_{i,-\sigma} \rangle$ and anti-ferro periodicity.

In Fig. 5, we show the calculated instability lines in the ζ - T plane for several values of Δ . The actual calculations were performed for $t_b \leq t_a$, but the results hold also for $t_a \leq t_b$, since on a bipartite lattice at half-filling the latter can be mapped on the former by exchange of a and b followed by the particle-hole transformation and the sign reversal of a and b operators on one sublattice. Several observations can be made. For the studied parameters there are two possible instabilities corresponding to the OO and OD modes. The OO mode, favored by more symmetric bands, is the leading instability over a broad range of band asymmetries. The OO instability is suppressed when one of the bands becomes narrow, in which case the instability line $T_{OO}(\zeta)$ extrapolates linearly to zero. The OD mode is the leading instability only for strongly asymmetric bands. For constant $t_a^2 + t_b^2$, the

$T_{OD}(\zeta)$ is insensitive to ζ within the accuracy of our calculation. For all ζ , the T_{OO} is less sensitive to the crystal field Δ than T_{OD} .

The OO instability shows little sensitivity to the presence of a charge gap in the disordered state as there is no apparent change in the behavior of $T_{OO}(\zeta)$ when the gap disappears. In Fig. 5, we mark closing of the charge gap above the LS state. The actual 1P spectral functions at temperatures just above T_c close to both ends of the ζ -range are shown in Fig. 1.

The results obtained for positive t_a and t_b can be readily extended to an arbitrary combination of $\pm t_a$, $\pm t_b$ by the transformation $c_i \rightarrow (-1)^i c_i$ ($c = a$ and/or b). This is because for $V_{1,2} = 0$ the orbital diagonal and orbital off-diagonal modes do not mix even within the same channel. The OD susceptibility $\chi_{OD}(\mathbf{q})$ is then insensitive to the signs of t_a and t_b , i.e. the OD divergence always takes place at (π, π) . The OO susceptibility $\chi_{OO}(\mathbf{q})$ is shifted by (π, π) if $t_a t_b < 0$, i.e. the OO divergence is at the zone center in this case.

For small non-zero cross hopping $V_{1,2}$ the location of the divergent modes are still determined by the signs of t_a and t_b . The main effect of such a finite $V_{1,2}$ is a partial lifting of the degeneracy of $\chi_{OO}(\mathbf{q})$, as shown in Fig. 3 for $V_{1,2} = 0.1$ eV. The $a_\sigma^\dagger b_{-\sigma}$ and $b_\sigma^\dagger a_{-\sigma}$ modes form symmetric and anti-symmetric combinations which follow distinct \mathbf{q} dependences. The degeneracy of $\uparrow\downarrow$ and $\downarrow\uparrow$ channels is not affected by the spin preserving hopping.

IV. DISCUSSION

Before discussing various limits of the studied model, we point out formal equivalence between the excitonic condensation and superconductivity. This can be seen by exchanging the notion of particle and hole for one of the fermionic species, e.g. $b_i \rightarrow b_i^\dagger$, which turns a - b repulsion into attraction. This equivalence obviously breaks down when electromagnetic response is concerned since the excitons carry no charge. Nevertheless, it is useful to consider the analogy to superconductivity, which is more familiar to most physicists. The excitonic order parameter in our study is local, i.e. has no \mathbf{k} -dependence, which is analogous to s -wave superconductivity. An $\langle ab \rangle$ order parameter, composed of different orbitals, is unusual for a superconductor, due to the weakness of the electron-electron attraction, but can be easily realized in an excitonic condensate, as the electron-hole attraction is strong. Consisting of two distinct orbitals, the spin part $\langle ab \rangle$ order parameter is not restricted by Pauli principle and can be both singlet or triplet. It is the $J > 0$ Hund's coupling which selects the triplet parameter in the studied model. Like for superconductivity, one may consider the strong-coupling (BEC) and the weak-coupling (BCS) limits.

A. Strong-coupling limit

The strong-coupling limit is characterized by the LS and HS states being separated from the remaining atomic states by energy $E_i - E_{\text{HS/LS}} \gg |t_a|, |t_b|, |V_{1,2}|$. In this case an effective model without charge fluctuations can be formulated using the Schrieffer-Wolff transformation²⁸, which provides a simplified picture of the low-energy physics. The resulting effective Hamiltonian with hopping treated to the second order is derived in Appendix A. In the following, we discuss some of its aspects.

1. Density-density interaction ($H_{\text{int}}^I = 0$)

First, we consider model (1) with the density-density interaction only for which the DMFT calculations, reported in preceding section, were performed. The effective Hamiltonian then has the form

$$H_{\text{eff}}^{\text{dd}} = \sum_i \mu n_i + K_\perp \sum_{ij,s} d_{i,s}^\dagger d_{j,s} + \sum_{\langle ij \rangle} (K_\parallel n_i n_j + K_0 S_i^z S_j^z) + K_1 \sum_{\langle ij \rangle, s} (d_{i,s}^\dagger d_{j,-s}^\dagger + d_{i,s} d_{j,-s}). \quad (2)$$

describing two flavors $s = \pm 1$ of bosons with the hardcore constraint $n_i = \sum_s d_{i,s}^\dagger d_{i,s} \leq 1$, corresponding to HS states created by $d_1^\dagger = a_\uparrow^\dagger b_\downarrow$ and $d_{-1}^\dagger = a_\downarrow^\dagger b_\uparrow$ out of the LS vacuum. Neglecting the cross-hopping contribution the coupling constants have a simple form $\mu = \Delta - 3J - Z \frac{t_a^2 + t_b^2}{U - 2J}$, $K_\perp = \frac{2t_a t_b}{U - 2J}$, $K_\parallel = (t_a^2 + t_b^2) \frac{U + 4J}{(U - 2J)(U + J)}$, and $K_0 = \frac{t_a^2 + t_b^2}{U + J}$, where $Z = 4$ is the number of nearest neighbors. The last term appears only for finite cross hopping and has the form $K_1 = -2V_1 V_2 \frac{U - 2J}{(U + J - \Delta)(U - 5J + \Delta)}$.

2. Classical limit ($\zeta = 0$)

The behavior of model (1) as revealed by the DMFT calculations strongly depends on the band asymmetry ζ . The OD instability was found only for rather asymmetric bands $t_a t_b \ll t_a^2 + t_b^2$, which leads to $K_\perp \ll K_\parallel$ in (2). In the limit $t_a t_b = 0$ the hopping K_\perp disappears, and the effective model (2) reduces to the classical Blume-Emmery-Griffiths (BEG) model²⁹. Assigning $s_i = 0$ to $|\text{LS}\rangle$ and $s_i = \pm 1$ to $d_{\pm 1}^\dagger |\text{LS}\rangle$ one arrives at its usual form

$$H_{\text{BEG}} = \mu \sum_i s_i^2 + \sum_{\langle ij \rangle} (K_\parallel s_i^2 s_j^2 + K_0 s_i s_j). \quad (3)$$

With our choice of the parameters U , J , $t_a^2 + t_b^2$ and Δ , we have $\mu \approx 0$ ($\mu = 0$ corresponds to $\Delta = 3.41$) and $K_\parallel / K_0 = 4$. According to Ref. 30, for $K_\parallel / K_0 = 4$ and μ between $\mu_{\text{min}} < 0 < \mu_{\text{max}}$ the BEG model exhibits a solid

(S) order, characterized by a checker-board arrangement of HS and LS sites. This is equivalent to a staggered density $\langle n_i \rangle$ in the language of the bosonic model (2). For $\mu < 0$ the order exists down to the zero temperature, for $\mu > 0$ the order disappears at finite T . The solid order as well as the reentrant transition was found also in previous DMFT simulations¹¹ of 2BHM with asymmetric bands. Proximity to the BEG limit thus provides a simple explanation of the OD instability in the strong coupling and asymmetric bands region of model (1). The analysis of the BEG model³⁰ suggests that for $\mu \approx \mu_{\min}$ competition between the anti-ferromagnetic and the solid phase gives rise to a rather complicated phase diagram. This parameter range is, however, beyond the scope of this work.

3. Superfluid phase

For general ζ , the hopping K_{\perp} cannot be neglected. Much studied in the context of cold atoms, the spinless version of (2) is known to host a superfluid (SF) phase in addition to the solid (S) phase discussed above. Existence of a supersolid order at the boundary between S and SF phases is a subject of intense research on the model generalizations³¹. The spinless model (2) can also be derived as the strong-coupling limit of the extended Falicov-Kimball model¹⁴.

The SF phase is characterized by a finite value of $\langle d_{i,s} \rangle$, which corresponds to spontaneous appearance of an off-diagonal expectation value $\langle a_{i,\sigma}^{\dagger} b_{i,-\sigma} \rangle$ in 2BHM, and thus can be identified with the observed OO instability. Without cross-hopping, $V_{1,2} = 0$, the SF phase of (2) is similar to the spinless case in the sense that it consists of two copies of the latter coupled only by amplitude fluctuations. Inclusion of the cross-hopping has a very different effect on the spinless and spinful models. In the spinless case¹⁴, the cross-hopping must have the same form as the d operator and thus non-zero V introduces a source term $V^*d + Vd^{\dagger}$ to the Hamiltonian, removing the distinction between the normal and SF phases. In the spinful case (2), however, the spin-preserving cross hopping has a different spin symmetry than the d_s operators and therefore non-zero V introduces the K_1 term instead. Finite K_1 locks together the phases of $\langle d_{i,1} \rangle$ and $\langle d_{i,-1} \rangle$. This is reflected in the partial lifting of the degeneracy of the OO mode. The distinction between the normal and SF phases is thus preserved irrespective of the cross hopping.

4. $SU(2)$ symmetric interaction

Next, we discuss the effect of the spin-flip and pair-hopping terms in H'_{int} , which were not included in the DMFT simulation. The spin-flip term renders model (1) $SU(2)$ symmetric and a third boson $d_0^{\dagger} = \frac{a_{\uparrow}^{\dagger} b_{\uparrow} - a_{\downarrow}^{\dagger} b_{\downarrow}}{\sqrt{2}}$ ap-

pears in the effective model

$$\begin{aligned}
H_{\text{eff}} = & \sum_i \mu n_i + K_{\perp} \sum_{ij} \mathbf{d}_i^{\dagger} \mathbf{d}_j \\
& + \sum_{\langle ij \rangle} (K_{\parallel} n_i n_j + K_0 \mathbf{S}_i \cdot \mathbf{S}_j) \\
& - K_1 \sum_{\langle ij \rangle} (\mathbf{d}_i^{\dagger} \cdot \mathbf{d}_j^{\dagger} + \mathbf{d}_i \cdot \mathbf{d}_j) \\
& + K_2 \sum_{i,j} (\mathbf{d}_i + \mathbf{d}_i^{\dagger}) \cdot \mathbf{S}_j.
\end{aligned} \tag{4}$$

Here, $(\mathbf{S}_i)_{\alpha} = \sum_{ss'} d_{i,s}^{\dagger} S_{ss'}^{\alpha} d_{i,s'}$ and $n_i = \sum_s d_{i,s}^{\dagger} d_{i,s}$, where $s = 0, \pm 1$ and $S_{ss'}^{\alpha}$ are spin $S=1$ operators. The d operators are arranged in a vector $\mathbf{d} = (\frac{1}{\sqrt{2}}(d_{-1} - d_1), \frac{1}{i\sqrt{2}}(d_{-1} + d_1), d_0)$. As before, the hard-core constraint $n_i \leq 1$ is assumed. We are not aware of any specific studies of the $S = 1$ model (4). On a mean field level one can repeat the arguments used for the density-density interaction which lead to the expectation of solid order for $K_{\perp} \ll K_{\parallel}$. The SF order parameter generalizes to a 3-component vector the phase of which is again determined by the K_1 term. The K_2 term is new and does not have an analogy in the density-density case.

5. Coupling constants

The full expressions for the coupling constants are given in Appendix A. Here, we consider their signs as functions the hopping parameters $t_{a,b}$ and $V_{1,2}$ and implications for the broken symmetry phases.

Varying the chemical potential $\mu \approx \Delta - 3J$, we can tune between two ‘trivial’ limits: the vacuum state $\langle n_i \rangle \approx 0$ for large Δ corresponding to the LS ground state of (1) and $\langle n_i \rangle \approx 1$ for small Δ , which corresponds to anti-ferromagnetic $S=1$ Heisenberg model. Our DMFT calculations fall into the intermediate Δ regime with non-integer $\langle n_i \rangle$.

The fact that K_{\parallel} is always positive, being proportional to $t_a^2 + t_b^2, V_1^2 + V_2^2$, implies that, irrespective of the signs of the hoppings, the OD instability leads always to an anti-ferro (AF) order. Similarly, $K_0 \sim t_a^2 + t_b^2, V_1^2 + V_2^2$ implies that there is always AF magnetic interaction between the nearest neighbors. The sign of $K_{\perp} \sim t_a t_b$ depends on the relative sign of t_a and t_b . The cross-hopping contribution to K_{\perp} is proportional to $V_1 V_2 J'$ and thus may interfere both constructively or destructively with the $t_a t_b$ term. $K_{\perp} > 0$ favors AF SF order while $K_{\perp} < 0$ favors ferro (F) SF order on a given bond. Therefore the OO divergence can be moved from (π, π) to $(0, 0)$ simply by changing the sign of t_a or t_b .

Non-zero K_1 fixes the phase of $\langle \mathbf{d} \rangle$ in the SF phase. Depending on the sign of $K_1 K_{\perp}$ it selects $\langle \mathbf{d} \rangle$ to be real or imaginary. This corresponds to divergence of either the symmetric $a^{\dagger} b + b^{\dagger} a$ or the anti-symmetric $a^{\dagger} b - b^{\dagger} a$ OO mode. The K_1 term appears when the pair-hopping $J' \neq$

0 or the cross-hopping $V_{1,2} \neq 0$ is present. Inspection of the formulas in Appendix A shows that for $V_{1,2} = 0$ the $K_1 \sim -J't_a t_b$ contribution always favors real $\langle \mathbf{d} \rangle$, while for $V_{1,2} \neq 0$ one can get either sign of $K_1 K_\perp$.

Finally, $K_2 \sim (V_1 t_a + V_2 t_b)$ appears only in the $SU(2)$ symmetric case with the cross-hopping present. In case of $\langle \mathbf{d} \rangle$ having a real component this term acts as an effective Zeeman field and induces spin polarization along $\langle \mathbf{d} \rangle$.

B. Weak-coupling limit

In the weak coupling limit, we consider almost empty (full) a (b) bands with a small mutual overlap and search for the divergencies of the static susceptibility using the random phase approximation. The bare susceptibility, in this case, is dominated by the diagonal elements $\chi_{ab,ab}^0$, corresponding to formation of electron-hole pairs with different orbital characters. The $\chi_{aa,aa}^0$ and $\chi_{bb,bb}^0$ elements, as well as $\chi_{aa,ab}^0$ which may appear due to the cross-hopping, are small and we can restrict our considerations to the 2×2 block of mixed orbital flavors. Depending on the sign of $t_a t_b$ the diagonal element $\chi_{ab,ab}^0$ is peaked either at $(0,0)$ or (π,π) due to Fermi surface nesting. If $V_{1,2} \neq 0$ an off-diagonal element $\chi_{ab,ba}^0$ appears.

We find divergent susceptibilities in the magnetic (triplet) channel which have the form

$$\chi_{OO}^{S,A} = \frac{\chi_{ab,ab}^0 \pm \chi_{ab,ba}^0}{1 - (U - 2J \pm J')(\chi_{ab,ab}^0 \pm \chi_{ab,ba}^0)} \quad (5)$$

and belong to a symmetric $a^\dagger b + b^\dagger a$ and an anti-symmetric $a^\dagger b - b^\dagger a$ mode, respectively. Positive J always favors χ_{OO}^S to be the leading divergence. The cross-hopping $V_{1,2}$, which controls the sign of $\chi_{ab,ba}^0$, may select χ_{OO}^S as well as χ_{OO}^A to be the leading instability. For $J' = V_{1,2} = 0$ the two modes are degenerate. Without Hund's coupling^{12,13,18,19} ($J = 0$) the singlet and triplet channels become degenerate. In that case, non-zero cross-hopping $V_{1,2}$ may preclude the phase transition in that the singlet excitonic pairing only enhances the existing off-diagonal expectation values. With Hund's coupling the triplet order parameter always represents a true symmetry breaking as it has distinct symmetry for an arbitrary spin-preserving hopping.

In the mean-field picture, assuming an F order for simplicity, we get

$$H_{MF} = \begin{pmatrix} \varepsilon_a(\mathbf{k})\sigma_0 & V(\mathbf{k})\sigma_0 + \boldsymbol{\sigma} \cdot \boldsymbol{\phi} \\ V^*(\mathbf{k})\sigma_0 + (\boldsymbol{\sigma} \cdot \boldsymbol{\phi})^* & \varepsilon_b(\mathbf{k})\sigma_0 \end{pmatrix}, \quad (6)$$

with σ_α being the Pauli matrices in the spin space. Divergence of χ_{OO}^S implies $\boldsymbol{\phi}^* = \boldsymbol{\phi}$ while divergence of χ_{OO}^A implies $\boldsymbol{\phi}^* = -\boldsymbol{\phi}$ (for details see Appendix B). Omitting the overall charge conservation, which is not broken at the transition, the order parameter reduces the $SU(2)$ symmetry of (1) into $U(1)$ and thus behaves as a point on

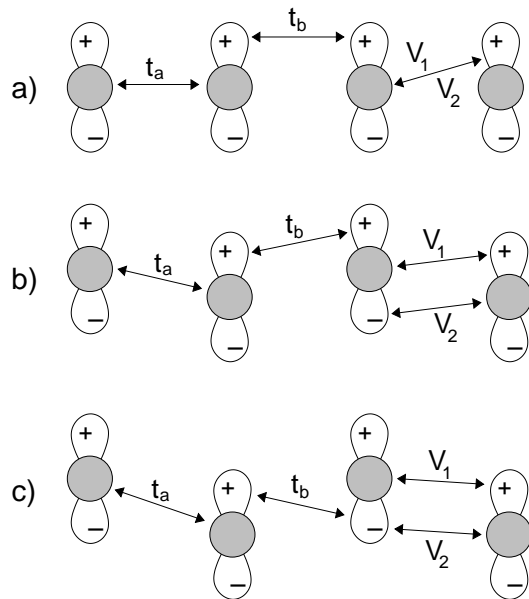


FIG. 6: An example of various combinations of the hoppings with orbitals of s and p_z symmetry. a) $t_{a,b} > 0$, $V_{1,2} = 0$, b) $t_{a,b} > 0$, $V_1 = -V_2$, and c) $t_a > 0$, $t_b < 0$, $V_1 = -V_2$.

S_2 sphere. If $J' = V = 0$ Hamiltonian (1) has additional $U(1)$ symmetry associated with the relative phase of a and b states. Breaking this symmetry leads to a complex order parameter that lives in $S_1 \times S_2$.

Expressions (5, 6) hold also in the case of density-density interaction with the provision that divergent $\chi_{OO}^{S,A}$ are found only in the $\uparrow\downarrow$ and $\downarrow\uparrow$ channels (not in $\uparrow\uparrow$ - $\downarrow\downarrow$) and $\phi_z \equiv 0$ in (6). The $SU(2)$ symmetry of Hamiltonian (1) reduces to $U(1)$ in case of the density-density interaction. The order parameter for non-zero $V_{1,2}$ is a real or imaginary vector (ϕ_x, ϕ_y) living in S_1 . If $V_{1,2} = 0$ the relative phases of all spin-orbital flavors are independent leading to $[U(1)]^3$ symmetry, which is reduced to $U(1)$ at the transition. The order parameter is then a complex vector (ϕ_x, ϕ_y) living in $S_1 \times S_1$.

C. Physical meaning of the excitonic order parameter

Finally, we discuss the physical meaning of the real, imaginary or complex excitonic order parameter. In Fig. 6 we present simple realizations of these phases using s and p_z orbitals: a) $V_{1,2} = 0$ with complex order parameter $\boldsymbol{\phi}$, b) $t_a t_b V_1 V_2 > 0$ with real $\boldsymbol{\phi}$ and c) $t_a t_b V_1 V_2 < 0$ with imaginary $\boldsymbol{\phi}$.

Let us start by considering real $\boldsymbol{\phi} = (0, 0, \phi_z)$. The corresponding operator $a_\uparrow^\dagger b_\uparrow - a_\downarrow^\dagger b_\downarrow + b_\uparrow^\dagger a_\uparrow - b_\downarrow^\dagger a_\downarrow$ describes the z -component of magnetization (spin) density with the distribution given by the product of a and b orbitals $\varphi_a(\mathbf{x})\varphi_b(\mathbf{x})$. In present case, the product is a p function, i.e. the leading multipole of the distribution is

a dipole and the above operator may be viewed as describing an on-site magnetic quadrupole. The rotation of ϕ corresponds to changing the magnetization direction while keeping its distribution fixed, i.e. cannot be viewed as a 3D rotation of the quadrupole as rigid object.

The operator $a_{\uparrow}^{\dagger}b_{\uparrow} - a_{\downarrow}^{\dagger}b_{\downarrow} - b_{\uparrow}^{\dagger}a_{\uparrow} + b_{\downarrow}^{\dagger}a_{\downarrow}$ corresponding to imaginary $\phi = (0, 0, \phi_z)$ describes an on-site pattern of a magnetization current. Rotation of imaginary ϕ corresponds to changing the magnetization direction while keeping the current pattern fixed. Complex ϕ is difficult to visualize. In this case it is possible to continuously rotate magnetic multipole into a local spin current without changing the energy of the system.

A model built on d_{z^2} and $d_{x^2-y^2}$ orbitals may be more realistic with respect to real materials. Similar considerations would apply leading to a finite value of magnetic octupole, in case of real, and more a complicated pattern of the on-site spin current, in case of imaginary order parameter. While the direct experimental detection of the magnetic multipoles may be experimentally difficult, presumably, the most experimentally accessible would be the effect of excitonic order on the transport properties at weak to moderate coupling.

D. Further work

Despite a narrow parameter range in the vicinity of the spin-state transition, the present results reveal a rich phase diagram, nevertheless, other phases may exist nearby. In the $\zeta = 0$ limit and Δ below the studied range, the BEG phase diagram contains anti-ferromagnetic HS phase separated from the solid HS-LS phase by a narrow strip of a phase containing both magnetic and HS-LS order. For finite ζ the boundary between the S and SF provides an interesting possibility for a stable super-solid phase. Although it was excluded for 2D spinless bosons^{20,21} with a simple nn repulsion, the effect of the additional terms in (4) or the departure from the strong-coupling limit is unexplored. Another interesting question is the possibility of coexistence of the SF and AF magnetic orders, observed in the bosonic t-J model with anisotropic exchange²³.

Our investigation of the Hubbard model in the vicinity of spin-state transition was motivated by the physics of LaCoO₃. While a two-band model ignoring the electron-lattice coupling is probably too simplistic to describe this complicated multi-orbital material, some useful insights are obtained. In particular, the present study shows that the excitonic condensation is in a broad range of parameters preferred to the HS-LS order, an order which has been discussed in LaCoO₃ context and treated with first-principles LDA+U method³². The proposal of excitonic condensation in this material may be tested on the same level of approximation by introducing the 'excitonic' instead of the standard mean-field decoupling of the on-site

interaction in LDA+U.

V. CONCLUSIONS

Using dynamical mean-field theory we have performed an unbiased numerical search probing all possible particle-hole instabilities of the two-band Hubbard model in the parameter range close to the spin-state transition. Our main result is the observation of an instability towards condensation of spinful excitons. Together with the previously reported solid HS-LS order, these are the only instabilities of the model in the studied parameter range. We have shown that keeping other parameters fixed the bandwidths ratio is the control parameter selecting the leading instability, an observation which has a particularly simple explanation in the strong coupling limit as tuning the ration of nn hopping and nn repulsion in a hard-core bosons model. The strong-coupling mapping onto spinful hard-core bosons with nn interaction provides a possibility of electronic realization of some exotic phases observed with cold atoms. Comparing the solid HS-LS order and the superfluid excitonic order we find that the former does not exist in the weak coupling regime and due to its Ising character can be easily suppressed by geometrical frustration, while the latter exists both in strong and weak coupling limits and due to the continuous character can better adapt to geometrical frustration, e.g. by forming a 120° order on triangular lattice. The main implication for real materials is the fact that the excitonic condensation should be considered a competitor to the HS-LS order in systems close to the spin-state transition.

Acknowledgments

We thank D. Vollhardt, A. Kampf, A. Kauch, P. Novák, R. T. Scalettar and J. Otsuki for discussions and valuable suggestions. We acknowledge the support of Deutsche Forschungsgemeinschaft through FOR1346 and the Grant Agency of the Czech Republic through project 13-25251S.

Appendix A: Strong coupling parameters

The parameters of the bosonic model were obtained by second order perturbation theory in the hopping using

$$(H_{\text{eff}})_{\alpha\beta} = \langle \alpha | H | \beta \rangle + \frac{1}{2} \sum_i \left(\frac{\langle \alpha | H | i \rangle \langle i | H | \beta \rangle}{E_{\alpha} - E_i} + \frac{\langle \alpha | H | i \rangle \langle i | H | \beta \rangle}{E_{\beta} - E_i} \right), \quad (\text{A1})$$

where $|\alpha\rangle$ and $|\beta\rangle$ are the states built from the local LS and HS states and $|i\rangle$ is everything else. The formula was evaluated in Mathematica using the SNEG package³³.

$$\begin{aligned}
\mu &= \Delta - 3J + Z(t_a^2 + t_b^2) \left(\frac{J'^2}{\Delta'^2 (U - 5J + 2\Delta')} - \frac{J'^2}{2\Delta'(\Delta' + \Delta)(U - 2J + \Delta' + \Delta)} - \frac{\Delta' + \Delta}{2\Delta'(U - 2J + \Delta' - \Delta)} \right) \\
&\quad + Z \frac{V_1^2 + V_2^2}{2} \left(\frac{J'^4}{\Delta'^2 (\Delta' + \Delta)^2 (U - 5J + 2\Delta' + \Delta)} - \frac{2}{U - 2J + \Delta'} + \frac{(\Delta' + \Delta)^2}{\Delta'^2 (U - 5J + 2\Delta' - \Delta)} \right) \\
K_{\parallel} &= (t_a^2 + t_b^2) \left(-\frac{J'^2}{\Delta'^2 (U - 5J + 2\Delta')} - \frac{J'^2}{(U + J)\Delta'(\Delta' + \Delta)} + \frac{J'^2}{\Delta'(\Delta' + \Delta)(U - 2J + \Delta' + \Delta)} \right. \\
&\quad \left. + \frac{\Delta'(U + J - \Delta) + \Delta(3J + \Delta)}{(U + J)\Delta'(U - 2J + \Delta' - \Delta)} \right) + \frac{V_1^2 + V_2^2}{2} \left(-\frac{J'^4}{\Delta'^2 (\Delta' + \Delta)^2 (U - 5J + 2\Delta' + \Delta)} + \frac{4}{U - 2J + \Delta'} \right. \\
&\quad \left. - \frac{(\Delta' + \Delta)^2}{\Delta'^2 (U - 5J + 2\Delta' - \Delta)} - \frac{2(U + J)}{(U + J)^2 - \Delta^2} \right) \\
K_{\perp} &= t_a t_b \left(\frac{J'^2}{\Delta'(\Delta' + \Delta)(U - 2J + \Delta' + \Delta)} + \frac{\Delta' + \Delta}{\Delta'(U - 2J + \Delta' - \Delta)} \right) + V_1 V_2 \frac{2J'}{\Delta'(U - 2J + \Delta')} \\
K_0 &= (t_a^2 + t_b^2) \frac{1}{U + J} + (V_1^2 + V_2^2) \frac{U + J}{(U + J)^2 - \Delta^2} \\
K_1 &= -t_a t_b \frac{2J'(U - 2J + \Delta')}{(U + J)\Delta'(U - 5J + 2\Delta')} - V_1 V_2 \left(\frac{J'^2 (U - 2J + \Delta' + \Delta)}{\Delta'(\Delta' + \Delta)(U + J + \Delta)(U - 5J + 2\Delta' + \Delta)} \right. \\
&\quad \left. + \frac{(\Delta' + \Delta)(U - 2J + \Delta' - \Delta)}{\Delta'(U + J - \Delta)(U - 5J + 2\Delta' - \Delta)} \right) \\
K_2 &= -\frac{V_1 t_a + V_2 t_b}{2\sqrt{2}\sqrt{\Delta'(\Delta' + \Delta)}} \left(J' \left(\frac{1}{U - 2J + \Delta'} + \frac{1}{U - 2J + \Delta' + \Delta} + \frac{1}{U + J + \Delta} + \frac{1}{U + J} \right) \right. \\
&\quad \left. + (\Delta' + \Delta) \left(\frac{1}{U - 2J + \Delta'} + \frac{1}{U - 2J + \Delta' - \Delta} + \frac{1}{U + J - \Delta} + \frac{1}{U + J} \right) \right),
\end{aligned}$$

where $\Delta' = \sqrt{\Delta^2 + J'^2}$. In Hamiltonian (1) we did distinguish between J in $H_{\text{int}}^{\text{dd}}$ and in H'_{int} . Nevertheless, the above expressions apply to both the models with density-density interaction $H_{\text{int}}^{\text{dd}}$ and the full interaction $H_{\text{int}}^{\text{dd}} + H'_{\text{int}}$ with the provision that in the density-density case $K_2 = 0$ and the other expressions are evaluated for $J' = 0$.

Appendix B: Mean-Field Decoupling

Here we show how a mean-field decoupling of the $(U - 2J) \sum_{\sigma} n_{a,\sigma} n_{b,-\sigma}$ term in the interaction gives rise to the spontaneous hybridization in the SF phase. First, we consider the $J' = V_{1,2} = 0$ case with degenerate $\chi_{\text{OO}}^{\text{S}}$ and $\chi_{\text{OO}}^{\text{A}}$ modes. Writing the above term as

$$-(U - 2J) (a_{\uparrow}^{\dagger} b_{\downarrow}) (b_{\downarrow}^{\dagger} a_{\uparrow}) - (U - 2J) (a_{\downarrow}^{\dagger} b_{\uparrow}) (b_{\uparrow}^{\dagger} a_{\downarrow}) \quad (\text{B1})$$

we obtain decoupling

$$\phi_1 a_{\uparrow}^{\dagger} b_{\downarrow} + \phi_1^* b_{\downarrow}^{\dagger} a_{\uparrow} + \phi_{-1} a_{\downarrow}^{\dagger} b_{\uparrow} + \phi_{-1}^* b_{\uparrow}^{\dagger} a_{\downarrow}, \quad (\text{B2})$$

using complex fields ϕ_1 and ϕ_{-1} , which acquire finite values

$$\phi_1 = \phi_x + i\phi_y \sim \langle b_{\downarrow}^{\dagger} a_{\uparrow} \rangle, \quad \phi_{-1} = \phi_x - i\phi_y \sim \langle b_{\uparrow}^{\dagger} a_{\downarrow} \rangle \quad (\text{B3})$$

in the SF phase.

If the $\chi_{\text{OO}}^{\text{S}}$ and $\chi_{\text{OO}}^{\text{A}}$ are not degenerate the fields ϕ_1 and ϕ_{-1} are not independent. In this case we use a decoupling which based on the symmetric and anti-symmetric modes starting from rewriting the interaction as

$$\begin{aligned}
& -\frac{U - 2J}{2} (a_{\uparrow}^{\dagger} b_{\downarrow} + b_{\uparrow}^{\dagger} a_{\downarrow}) (a_{\downarrow}^{\dagger} b_{\uparrow} + b_{\downarrow}^{\dagger} a_{\uparrow}) - \\
& \frac{U - 2J}{2} (a_{\uparrow}^{\dagger} b_{\downarrow} - b_{\uparrow}^{\dagger} a_{\downarrow}) (b_{\downarrow}^{\dagger} a_{\uparrow} - a_{\downarrow}^{\dagger} b_{\uparrow}) \quad (\text{B4})
\end{aligned}$$

leading to a decoupling

$$\begin{aligned}
& \phi_S (a_{\uparrow}^{\dagger} b_{\downarrow} + b_{\uparrow}^{\dagger} a_{\downarrow}) + \phi_S^* (a_{\downarrow}^{\dagger} b_{\uparrow} + b_{\downarrow}^{\dagger} a_{\uparrow}) + \\
& \phi_A (a_{\uparrow}^{\dagger} b_{\downarrow} - b_{\uparrow}^{\dagger} a_{\downarrow}) + \phi_A^* (b_{\downarrow}^{\dagger} a_{\uparrow} - a_{\downarrow}^{\dagger} b_{\uparrow}) \quad (\text{B5})
\end{aligned}$$

with

$$\phi_S \sim \langle a_{\downarrow}^{\dagger} b_{\uparrow} + b_{\downarrow}^{\dagger} a_{\uparrow} \rangle, \quad \phi_A \sim \langle b_{\downarrow}^{\dagger} a_{\uparrow} - a_{\downarrow}^{\dagger} b_{\uparrow} \rangle. \quad (\text{B6})$$

Comparing the corresponding terms in H_{MF} we see that finite ϕ_S implies $\phi_1 = \phi_{-1}^*$ and thus real ϕ_x and ϕ_y . Finite ϕ_A on the other hand implies $\phi_1 = -\phi_{-1}^*$ and thus imaginary ϕ_x and ϕ_y .

Since the decoupled term appears in both the $SU(2)$ and density-density interactions the above derivations

applies to both cases. In the $SU(2)$ interaction, which includes the spin-flip term, decoupling in terms of $a_{\uparrow}^{\dagger}b_{\uparrow} - a_{\downarrow}^{\dagger}b_{\downarrow}$ is possible, which leads to the same mean-field equa-

tions and gives rise to the ϕ_z component of the order parameter.

-
- ¹ A. Georges, L. de' Medici, and J. Mravlje, *Annu. Rev. Condens. Matter Phys.* **4**, 137 (2013).
- ² Z. P. Yin, K. Haule, and G. Kotliar, *Nat. Phys.* **7**, 294 (2011).
- ³ J. Kuneš, A. V. Lukoyanov, V. I. Anisimov, R. T. Scalettar, and W. E. Pickett, *Nat. Mater.* **7**, 198 (2008).
- ⁴ J. Kuneš, D. M. Korotin, M. A. Korotin, V. I. Anisimov, and P. Werner, *Phys. Rev. Lett.* **102**, 146402 (2009).
- ⁵ V. Křápek, P. Novák, J. Kuneš, D. Novoselov, D. M. Korotin, and V. I. Anisimov, *Phys. Rev. B* **86**, 195104 (2012).
- ⁶ R. Eder, *Phys. Rev. B* **81**, 035101 (2010).
- ⁷ P. Augustinský and J. Kuneš, *Computer Physics Communications* **184**, 2119 (2013).
- ⁸ J. Chaloupka and G. Khaliullin, *Phys. Rev. Lett.* **110**, 207205 (2013).
- ⁹ P. Werner and A. J. Millis, *Phys. Rev. Lett.* **99**, 126405 (2007).
- ¹⁰ R. Suzuki, T. Watanabe, and S. Ishihara, *Phys. Rev. B* **80**, 054410 (2009).
- ¹¹ J. Kuneš and V. Křápek, *Phys. Rev. Lett.* **106**, 256401 (2011).
- ¹² B. I. Halperin and T. M. Rice, *Rev. Mod. Phys.* **40**, 755 (1968).
- ¹³ L. Balents and C. M. Varma, *Phys. Rev. Lett.* **84**, 1264 (2000).
- ¹⁴ C. D. Batista, *Phys. Rev. Lett.* **89**, 166403 (2002).
- ¹⁵ B. Zenker, D. Ihle, F. X. Bronold, and H. Fehske, *Phys. Rev. B* **85**, 121102 (2012).
- ¹⁶ B. Zenker, D. Ihle, F. X. Bronold, and H. Fehske, *Phys. Rev. B* **83**, 235123 (2011).
- ¹⁷ K. Seki, R. Eder, and Y. Ohta, *Phys. Rev. B* **84**, 245106 (2011).
- ¹⁸ B. Zocher, C. Timm, and P. M. R. Brydon, *Phys. Rev. B* **84**, 144425 (2011).
- ¹⁹ T. Kaneko, K. Seki, and Y. Ohta, *Phys. Rev. B* **85**, 165135 (2012).
- ²⁰ G. Schmid, S. Todo, M. Troyer, and A. Dorneich, *Phys. Rev. Lett.* **88**, 167208 (2002).
- ²¹ G. G. Batrouni and R. T. Scalettar, *Phys. Rev. Lett.* **84**, 1599 (2000).
- ²² A. Kuklov, N. Prokof'ev, and B. Svistunov, *Phys. Rev. Lett.* **92**, 050402 (2004).
- ²³ M. Boninsegni and N. V. Prokof'ev, *Phys. Rev. B* **77**, 092502 (2008).
- ²⁴ A. Georges, G. Kotliar, W. Krauth, and M. J. Rozenberg, *Rev. Mod. Phys.* **68**, 13 (1996).
- ²⁵ W. Metzner and D. Vollhardt, *Phys. Rev. Lett.* **62**, 324 (1989).
- ²⁶ P. Werner, A. Comanac, L. de' Medici, M. Troyer, and A. J. Millis, *Phys. Rev. Lett.* **97**, 076405 (2006).
- ²⁷ E. Gull, A. J. Millis, A. I. Lichtenstein, A. N. Rubtsov, M. Troyer, and P. Werner, *Rev. Mod. Phys.* **83**, 349 (2011).
- ²⁸ J. R. Schrieffer and P. A. Wolff, *Phys. Rev.* **149**, 491 (1966).
- ²⁹ M. Blume, V. J. Emery, and R. B. Griffiths, *Phys. Rev. A* **4**, 1071 (1971).
- ³⁰ W. Hoston and A. N. Berker, *Phys. Rev. Lett.* **67**, 1027 (1991).
- ³¹ F. Mila, J. Dorier, and K. P. Schmidt, *Prog. Theor. Phys. Supplement* **176**, 355 (2008).
- ³² K. Křížek, Z. Jiráček, J. Hejtmánek, P. Novák, and W. Ku, *Phys. Rev. B* **79**, 014430 (2009).
- ³³ R. Žitko, *Comput. Phys. Commun.* **182**, 2259 (2011).